COMPARATIVE STUDY OF PHOTOCATALYTIC ACTIVITY IN NANOSCALE TiO_2 –M_xO_y (WHERE M=Co, Cu, Ru) HETEROSTRUCTURES

M.B Nayan[1], K. Jagadish[2], K. Namratha[3] and S. Srikantaswamy[4*]

[1]Research Scholar, Department of Studies in Environmental Science, University of Mysore, Manasagangothri, Mysuru-570006, India

[2]Assistant Professor, Department of Chemistry, Yuvaraja College, University of Mysore, Mysuru-570005, India.

[3]Research Associate, Center for Materials Science and Technology, Vijnana Bhavana, & Department of Studies in Earth Science, University of Mysore, Manasagangothri, Mysuru-570006, India

[4]Professor, Department of Studies in Environmental Science, University of Mysore, Manasagangothri, Mysuru-570006, India

Corresponding Author, Professor and Coordinator, Center for Materials Science and Technology, Vijnana Bhavana, University of Mysore, Manasagangothri, Mysuru-570006, India, Email: srikantas@hotmail.com

Abstract:

TiO_2–M_xO_y heterostructures (M=Co, Cu, or Ru) have been synthesized via facile hydrothermal route. The products have been characterized using powder x-ray diffraction (XRD), scanning electron microscopy (SEM), energy-dispersive powder X-ray spectroscopy (EDX), and UV-visible diffusive reflectance spectroscopy (UV-Vis DRS). Solar driven photocatalytic activity carried out through the degradation of 4-chlorophenol (4-CP) under natural sunlight irradiation. The effects of chemical composition, band gap, and charge carrier transport pathway have been investigated and established Z-scheme charge carrier transport pathway. It is found that the charge carriers transport pathway plays a more important role than band gap and light absorption in the photocatalysis process.

Keywords: TiO_2 -M_xO_y heterostructures; Solar driven photocatalyst; Charge carrier transport pathway; Z-scheme.

Introduction:

Photocatalytic degradation is a promising green technology to remove pollutants from water. TiO_2 is a standard photocatalyst extensively studied by a large number of researchers [1-2]. However, pristine TiO_2 is unable to absorb visible light due to its large band gap (3.2 eV) which limits its sunlight and visible light utilization. The high recombination rate of photogenerated electrons and holes negatively affect its photocatalytic activity [3].

Recently, several effort have been made to overcome these limitations including surface modification, morphology engineering, intrinsic and extrinsic doping, sensitizing and so on. [4,5] In this context, heterostructure approach has attracted attention of researchers because it can highly reduce the charge recombination rate significantly. For example, $SrTiO_3/TiO_2$ [6], SnO_2-TiO_2 [7], NiO-TiO_2 [8] showed higher photocatalytic activity than pure TiO_2 which was attributed to the higher charge carrier separation.

Moreover, metal oxides and metal sulfides heterostructure approach can extend the light absorption of TiO_2 to the visible light region by coupling it with an appropriate semiconductor with a narrow band gap [9-10]. Various visible light/ sunlight driven TiO_2-M_xO_y and TiO_2-M_xO_y (where M= Co, Cu, Ru, Bi, Ce)

heterostructures photocatalysts have been introduced and practiced for pollutant degradation such as Cu_2O/TiO_2, Bi_2O_3/TiO_2 and $ZnMn_2O_4/TiO_2$ [11], MoS_2-TiO_2[12], Co_3O_4-TiO_2 [13,14], RuO_2-TiO_2[15] and CuO-TiO_2[16]. However, most of these heterostructures are heterojunctions, in which the charge separation is highly enhanced but the photoinduced electrons and holes migrate to the corresponding conduction band (CB)/ valence band (VB) which negatively affect their redox potential [17].

Therefore, direct Z-scheme is an ideal approach to overcome the drawbacks of heterojunction [18]. Fabrication of an ideal Z-scheme TiO_2-based heterostructure can be achieved by choosing an appropriate semiconductor narrow band gap/ having conduction band minimum (CBM) higher than the redox potential of $O_2/^{\bullet}O_2$ (-0.046 V vs NHE)[19,20]. The best example of direct Z-scheme is TiO_2-g-C_3N_4 which exhibit a drastic enhancement in the sunlight photocatalytic activity because of the strong redox potential and extended light absorption [21].

Herein, we investigate the effect of charge migration pathway in TiO_2- based heterostructure along with the band gap. TiO_2-Co_3O_4, RuO_2-TiO_2, and CuO-TiO_2 have been fabricated via facile hydrothermal synthesis method. The solar driven photocatalytic activity has been examined by monitoring the degradation of 4-CP under sunlight irradiation. The conduction band minimum (CBM) and valence band maximum (VBM) of pristine TiO_2, RuO_2, CuO, Co_3O_4, was calculated from Tauc's plot. A possible mechanism was been proposed.

Experimental Methodology:

Materials:

Regents grade potassium titanium oxalate (98 %, Sigma Aldrich), $Co(NO_3)_2.6H_2O$ (99%, Alfa Aesar) USA, $Cu(NO_3)_2{\cdot}3H_2O$ (97%, Loba Chemie) India, and $Ru(NO)(NO_3)_3$ (98 %, Merck) Germany were used as raw materials.

Synthesis procedure:

Synthesis of anatase TiO_2 nanoparticles:

In a typical synthesis, 1.4 g of potassium titanium oxalate (PTO) was dissolved in 30 mL deionized water, followed by the addition of 30 mL 30% H_2O_2 and 0.8 mL of 37% HCl. The solution was then transferred to a 100 mL Teflon-lined autoclave. The hydrothermal synthesis was carried out at 150 ˚C for 24 h, and allowed to cool to room temperature naturally. The white precipitates was collected by means of centrifugation, washed several times with deionized water and ethanol, then dried in vacuum at 80 ◦C for 8 h and calcined in air at 400 ºC.

Synthesis of of TiO_2 –Co_3O_4 , TiO_2-RuO_2, and TiO_2-CuO heterostructure:

About 1.4 g of PTO was dissolved in 30 mL deionized water, followed by the addition of 30 mL 30% H_2O_2 and 0.8 ml of 37% HCl. About 2g of $Co(NO_3)_2$ 6 H_2O was added to the solution and stirred for 30 min. The solution was then transferred to a 100 mL Teflon-lined autoclave. The hydrothermal synthesis was carried out at 150˚C for 24 h, and was allowed to cool to room temperature naturally. The product was collected by means of centrifugation, washed several times with deionized water and ethanol, then dried in a vacuum at 60˚C for 8 h and calcined in air at 400ºC for 2 h.

The same procedure was used to synthesized CuO-TiO_2 and RuO_2-TiO_2 by replacing $Co(NO_3)_2.6H_2O$ by $Cu(NO_3)_2{\cdot}3H_2O$, and $Ru(NO)(NO_3)_3$.

Characterizations:

The heterostructures synthesized were characterized using a Rigaku Smart Lab–II powder X-ray diffractometer (XRD) with a, CuKα radiation (λ= 1.540598 Å), a Hitachi scanning electron microscope (SEM, Hitachi S3400N), a JASCO 460 Plus FTIR spectrometer, and a Shimadzu UV-2450 spectrophotometer (UV-Vis DRS).

Photocatalytic test:

The photocatalytic properties of as synthesized pristine TiO_2 and TiO_2–based heterostructures were carried out by monitoring the degradation of 4-chlorophenol (4-CP) under solar light irradiation. About 0.5 g of the photocatalyst was dispersed in 200 ml 4-CP (10 mg/L). The suspension was stirred for 4 min in the dark prior to the photocatalytic reaction. Then the suspension was exposed to natural sunlight irradiation for 80 min with magnetically stirring. About 3 mL of the suspension was sampled at every 20 min and subjected to centrifugation to remove the photocatalyst. A Beckman Coulter DU 730 UV−Vis spectrophotometer was used to measure the concentration of 4-CP.

Results and discussion:

XRD analysis:

Fig.1 shows powder XRD patterns of TiO_2-Co_3O_4, TiO_2-CuO, TiO_2-RuO_2, and pristine TiO_2. The pure TiO_2 exhibits reflections at 2θ = 25.61, 36.82, 37.60, 38.53, 48.22, 53.92, 55.81, 62.43, and 68.43° characteristic of the (101), (103), (004), (112), (200), (105), (211), (213), and (116) planes respectively of anatase TiO_2 phase (JCPDS-00-021-1272). The additional reflections observed in the pattern of TiO_2-Co_3O_4 are corresponding to the cubic Co_3O_4 (JCPD 78-1970) (JCPDS 43-1003) [22]. The characteristic peaks of CuO are observed at 32.23 and 35.23° on the pattern of CuO-TiO_2 (JCPDS 00-002-1040)[23-25] The peaks at 28.0, 35.1 on the pattern correspond to RuO_2 (JCPDS 43-1027 [26].

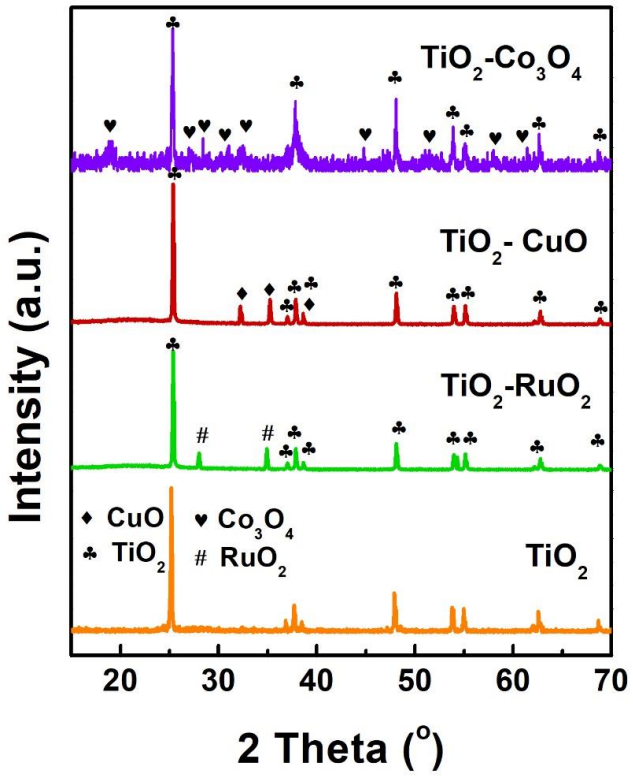

Fig.1 XRD patterns of the as prepared TiO_2 – Mx Oy heterostructures

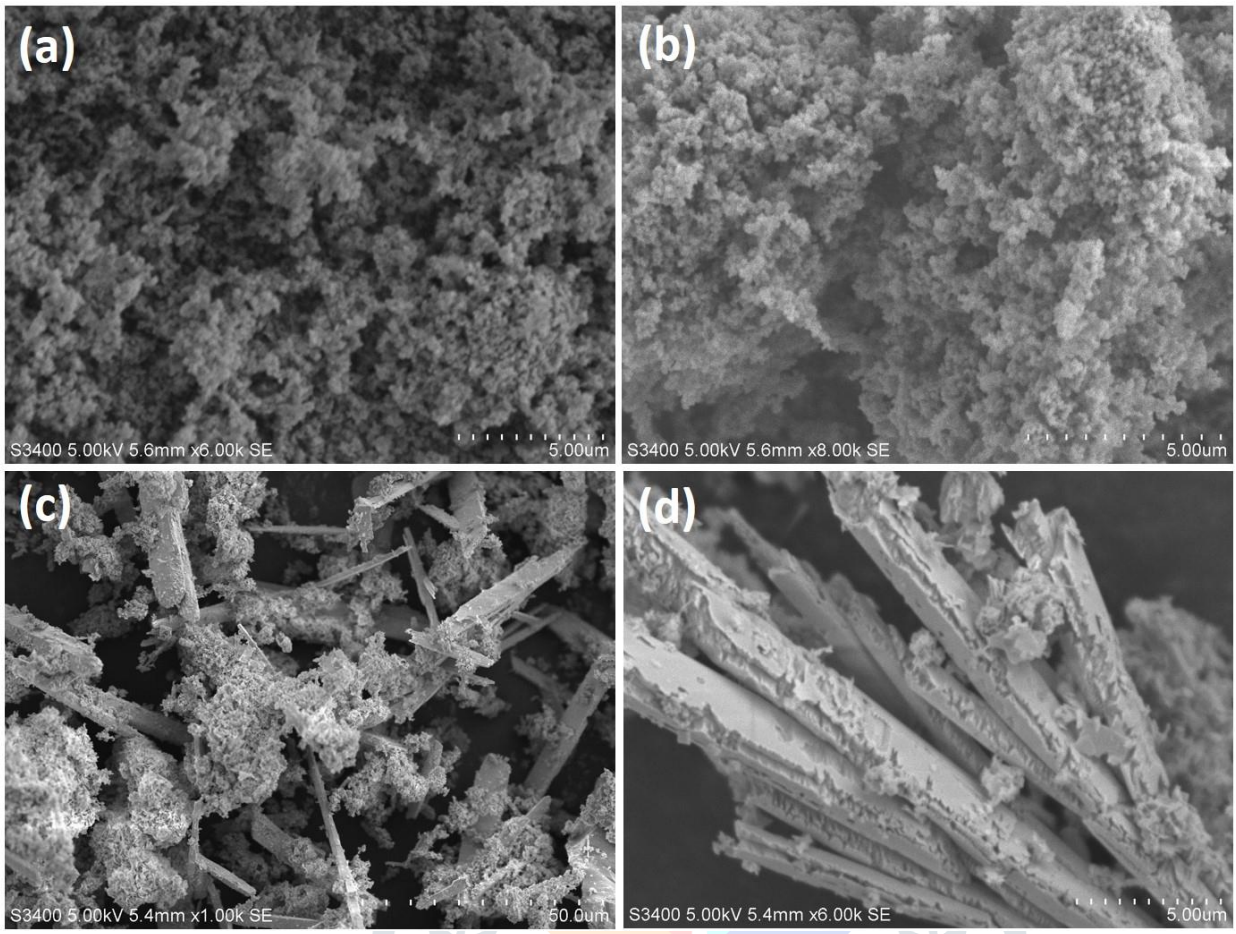

Fig. 2. SEM images of CuO-TiO_2, (b) Co_3O_4-TiO_2, and (c, d) RuO_2-TiO_2

SEM analysis:

Fig. 2 shows the morphology of as-prepared CuO-TiO_2, Co_3O_4-TiO_2, and RuO_2-TiO_2 heterostructures. It can be seen that CuO-TiO_2 and Co_3O_4-TiO_2 consist of agglomeration of small nanoparticles of no particular shape with an interlocked porous structures. RuO_2-TiO_2 exhibits fractured lath-like structure covered with agglomeration of nanoparticles (Fig. 2c,d).

EDX analysis:

To further confirm the formation of CuO-TiO_2, Co_3O_4-TiO_2, and RuO_2-TiO_2 heterostructures, EDX analysis was carried out and the results are shown in Fig.3. The characteristic peaks of Ti, Cu, and O appear in the spectrum of CuO-TiO_2. The peaks of Carbon appears due to the carbon tape used in the SEM sample holder. Only Ti, O, and Co, peaks appear in the EDX spectrum of Co_3O_4-TiO_2 confirming its formation and purity. The EDX spectrum of RuO_2-TiO_2 also confirm its successive formation. The details of EDX analysis is presented in Table 1.

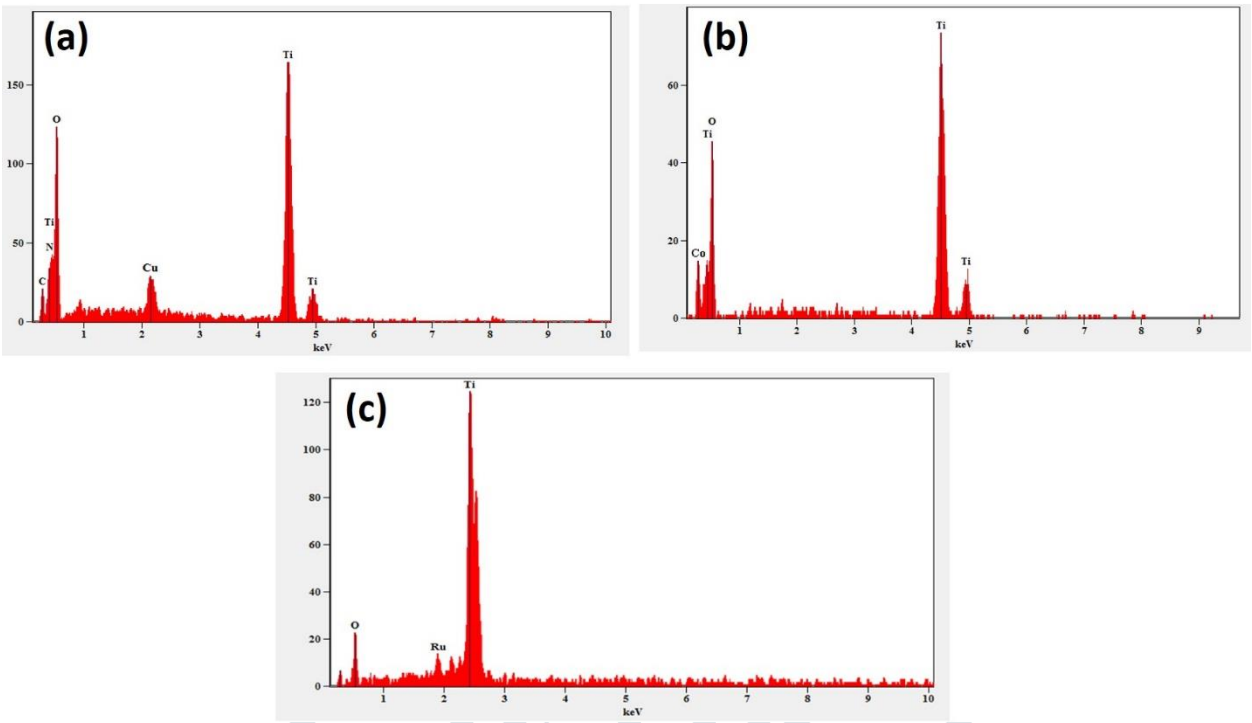

Fig. 3 EDX spectra of (a) CuO-TiO_2, (b) Co_3O_4-TiO_2, and (c) RuO_2-TiO_2.

Table 1. Elemental Analysis of CuO-TiO_2, Co_3O_4-TiO_2, and RuO_2-TiO_2 Heterostructures

Element Line	***Weight %***	***Weight % Error***	***Atom %***
CuO-TiO_2			
C K	22.60	±1.89	40.48
N K	0.00	----	0.00
O K	28.915	-----	38.88
Ti K	43.28	±1.24	19.44
Ti L	----	----	---
Cu L	5.21	±0.51	1.21
Total	100.00		100.00
TiO_2-Co_3O_4			
Co K	30.03	± 2.74	48.76
O K	28.02	---	34.16
Ti K	41.95	± 1.82	17.08
Ti L	---	---	---
Total	100.00		100.00
TiO_2-RuO_2			
Ru K	19.43	± 2.78	41.61
O K	27.80	± 2.55	44.68
Ti L	52.77	± 3.43	13.72
Total	100.00		100.00

FT-IR analysis:

FT-IR spectra of TiO_2-Co_3O_4, TiO_2-CuO, and TiO_2-RuO_2 heterostructures, and pure TiO_2 are shown in Fig.4. The fingerprint of metal oxygen bonds present in all heterostructure in the range of 450- 650 cm^- [27]. The broad bands appear near 1630 cm^{-1} and 3445 cm^{-1} correspond to the bending and stretching O-H vibration of water molecules adsorbed from the atmosphere on the surface of heterostructures while handling the samples in air for FT-IR studies. The absorption peak in the 1402 cm^{-1} indicates the presence of CO_2 from the atmospheric adsorption [28].

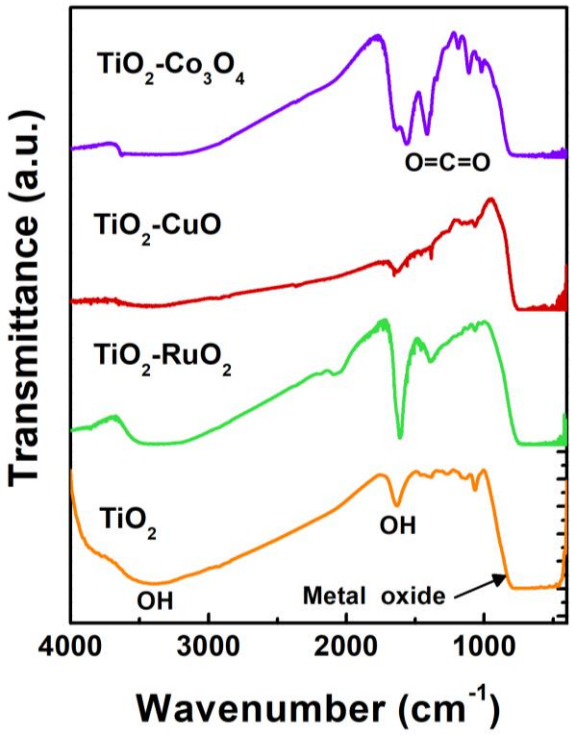

Fig.4. FTIR spectra of as-prepared TiO_2-Co_3O_4, TiO_2-CuO, and TiO_2-RuO_2 heterostructures.

Photocatalytic Studies:

The photocatalytic activity of the heterostructures prepared was investigated using 4-CP as a colorless model to avoid the sensitization effect and hence to accurately estimate the photocatalytic activity of the various heterostructures [29]. Fig. 5a shows the photodegradation curves over various TiO_2-based heterostructures as a function of irradiation time. No remarkable removal of 4-CP was detected after 40 min of magnetic stirring in the dark. It can be seen that about 85 % of 4-CP was degraded over TiO_2-CuO in the first 20 min of sunlight irradiation while, only 49%, 38%, and 15% was degraded respectively over, Co_3O_4-TiO_2, RuO_2-TiO_2, and pristine TiO_2. CuO-TiO_2 showed the higher photocatalytic degradation efficiency and about 97% of 4-CP was degraded in 80 min of sunlight irradiation. Figure 5b show that CuO-TiO_2, Co_3O_4-TiO_2, RuO_2-TiO_2, and pristine TiO_2 is first-order reaction and the reaction constant (k) is 0.02971, 0.0092, 0.00585, and 0.0048 for TiO_2-CuO, TiO_2-Co_3O_4, TiO_2-RuO_2, TiO_2, respectively. Thus, the photocatalytic activity follows the trend of TiO_2-CuO>> TiO_2-Co_3O_4> TiO_2-RuO_2 > TiO_2. Obviously, all heterostructures exhibit higher photocatalytic performance than the pristine TiO_2 confirming the impact of heterostructure fabrication. The mechanism behind the variation in photocatalytic activity of various heterostructures is investigated in the next section.

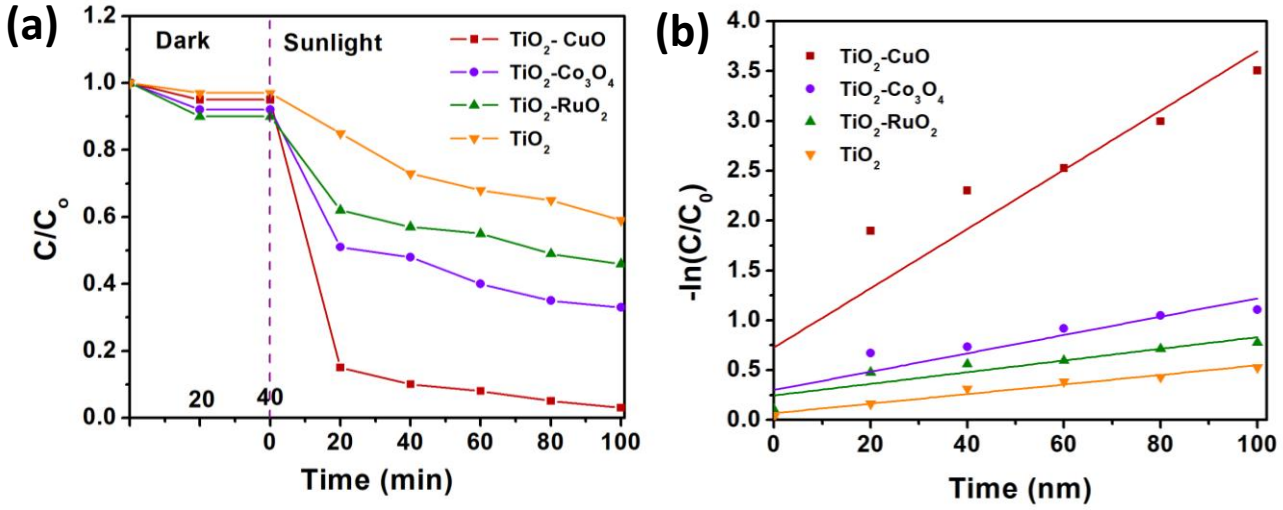

Fig. 5 (a) Photodegradation curves, and (b) kinetics of the photodegradation.

Charge transfer pathway and photodegradation mechanism:

Estimating the CBM and VBM is vital to understand the mechanism of photocatalytic degradation of the photocatalyst. To estimate CBM and VBM of the heterostructures components, UV-vis DRS spectra of TiO_2, CuO, Co_3O_4, and RuO_2 were recorded and presented in Fig. 6. Tauc's plot of each semiconductor was derived from the respective UV-Vis DRS spectrum and is presented in Fig. 6 (insets). The indirect band gap (E_g) of TiO_2 is 3.1 eV while the direct band gaps of CuO, RuO_2, and Co_3O_4 are 1.35, 2.25, and 2.09 eV respectively. The CBM and VBM are calculated from the following equations [30,31]

$CBM = \chi - E_H - 0.5E_g$

$VBM = CBM + E_g$

Where, χ is the electronegativity which equals 5.81, 6.35 [15], 5.93 [32], and 4.32 eV [33]for TiO_2, RuO_2, Co_3O_4, and CuO respectively, and E_H represents the energy of free electrons on the hydrogen scale (4.5 eV). The calculated CBM and VBM for pristine TiO_2, RuO_2, Co_3O_4, and CuO are presented in Table 2.

Table 2 CBM and VBM values.

	x	Eg	CBM	VBM
TiO_2	5.81	3.1	-0.24	2.86
RuO_2	6.35	2.25	0.73	2.975
CuO	4.32	1.35	-0.86	0.495
Co_3O_4	5.93	2.09	0.39	2.475

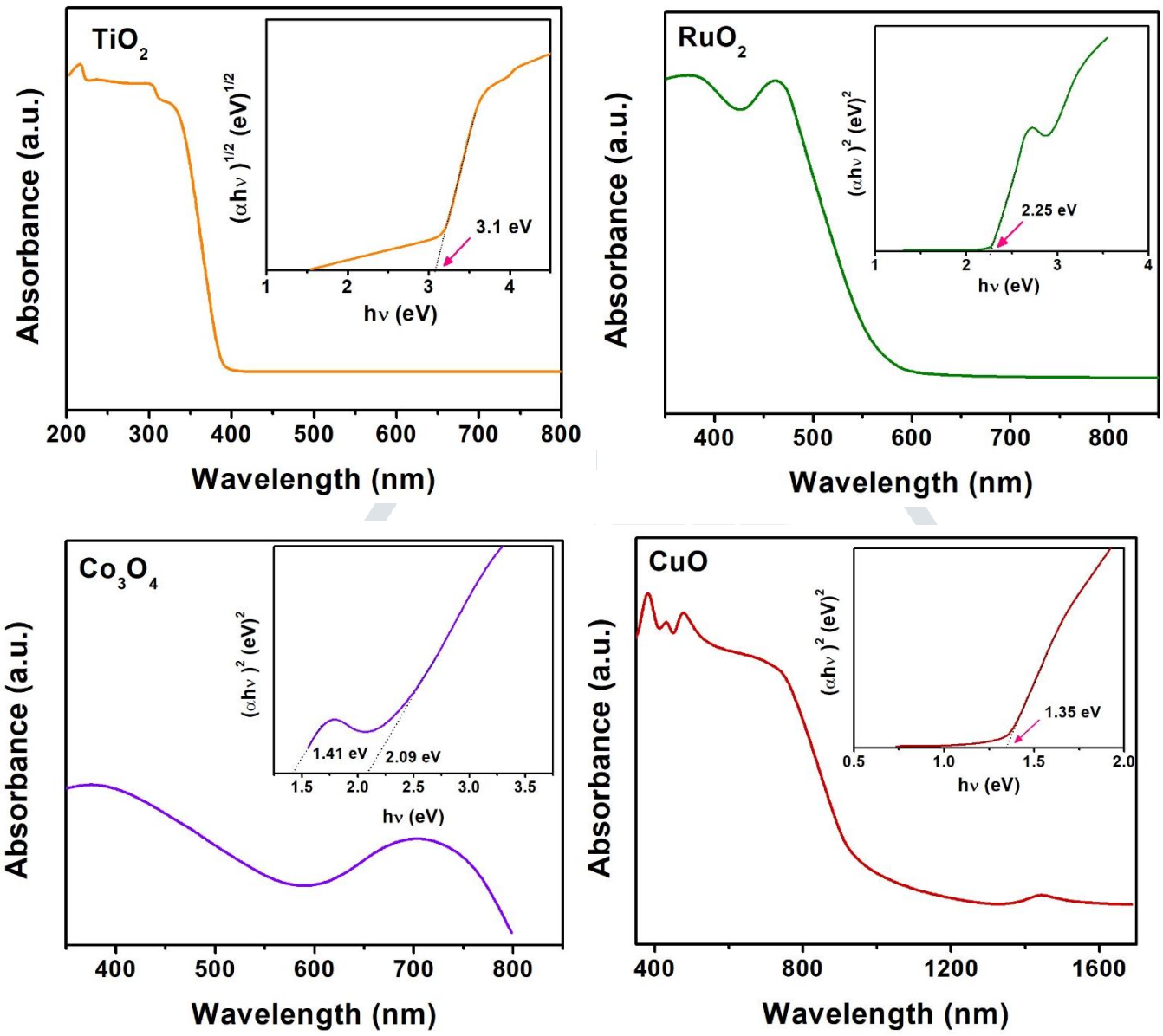

Figure 6. UV-vis DRS spectra and Tacu plots of pristine TiO_2, RuO_2, Co_3O_4, and CuO.

Based on these calculations the bands positions diagram was represented in Scheme 1. It can be seen that CBM and VBM of CuO-TiO_2 are suitable to construct a direct Z-scheme system. Therefore, under irradiation the photogenerated electrons in the CB of TiO_2 combine with the holes in the VB of CuO. Then they will not stop there but under irradiation they will be excited to the CB of CuO. The potential at CBM of CuO (-0.86 V vs NHE) is higher than the redox potential required to reduce O_2 into $^{\bullet}O_2$. The holes remain in the VB of TiO_2 which it has enough potential to produce $^{\bullet}OH$. $^{\bullet}OH$ and $^{\bullet}O_2$ degrade the 4-CP.

In contrast, the CBM and VBM of RuO_2 and Co_3O_4 are not suitable to construct Z-scheme systems with TiO_2 but they form RuO_2-TiO_2 and Co_3O_4-TiO_2 heterojunctions. Therefore during the irradiation, the photogenerated electrons migrate to the CB of RuO_2 (0.73 V vis NHE) and CB of Co_3O_4 (0.39 V vis NHE) which do not have enough redox potential to reduce O_2 into $^{\bullet}O_2$. Thus in RuO_2-TiO_2 and Co_3O_4-TiO_2 heterojunctions only $^{\bullet}OH$ is produced therefore, they exhibit lower photocatalytic activity than CuO –TiO_2.

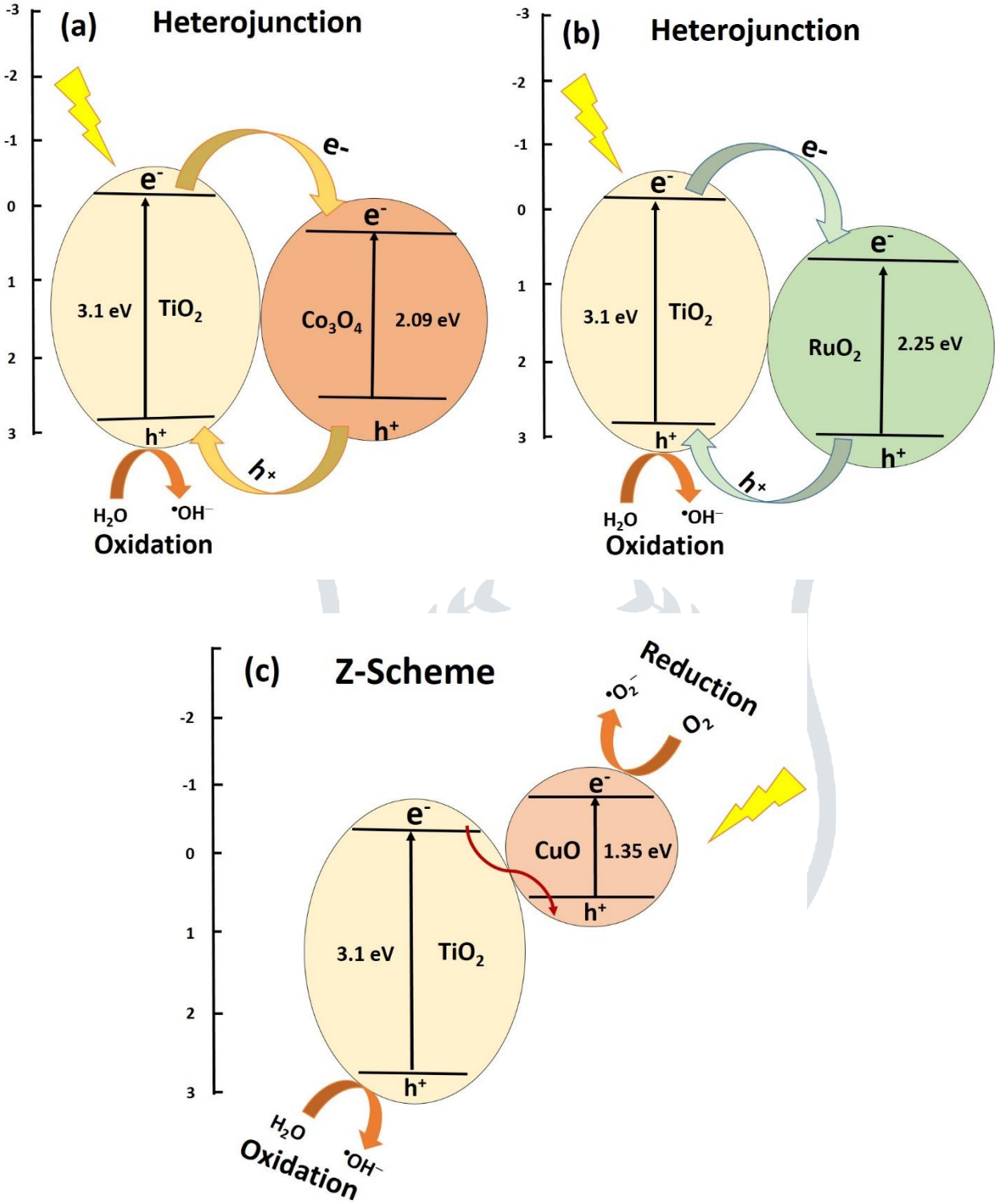

Scheme. 1 Mechanism of charge carrier pathway and photodegradation process.

Mechanism evidence:

To prove the proposed mechanism and to identify the main active species responsible for the photodegradation, tert-butyl alcohol (TBA) was used as an •OH scavenger and benzoquinone (BQ) as an $•O_2$ scavenger [20]. Fig.7 shows the effect of TBA and BQ on the 4-CP photodegradation over the synthesized heterostructures. In can be seen that in the presence of TBA the photocatalytic activity if three heterostructures decreased. This confirms the production of •OH during the photocatalytic process by each of the fabricated heterostructures. While in the presence of BQ only the photocatalytic activity of CuO-TiO_2 heterostructure is affected confirming the production of $•O_2$ by CuO-TiO_2 only and no $•O_2$ is produced by Co_3O_4-TiO_2 or RuO_2-TiO_2. In fact, this supports the proposed mechanism, that the photogenerated electrons migrate to CBM of CuO through Z-scheme pathway. CBM of CuO has enough redox potential to reduce O_2 and produce $•O_2$. While in the case of Co_3O_4-TiO_2 or RuO_2-TiO_2 the photogenerated electrons migrate to CBM of Co_3O_4 and RuO_2 respectively which they don't have enough redox potential to reduce $•O_2$.

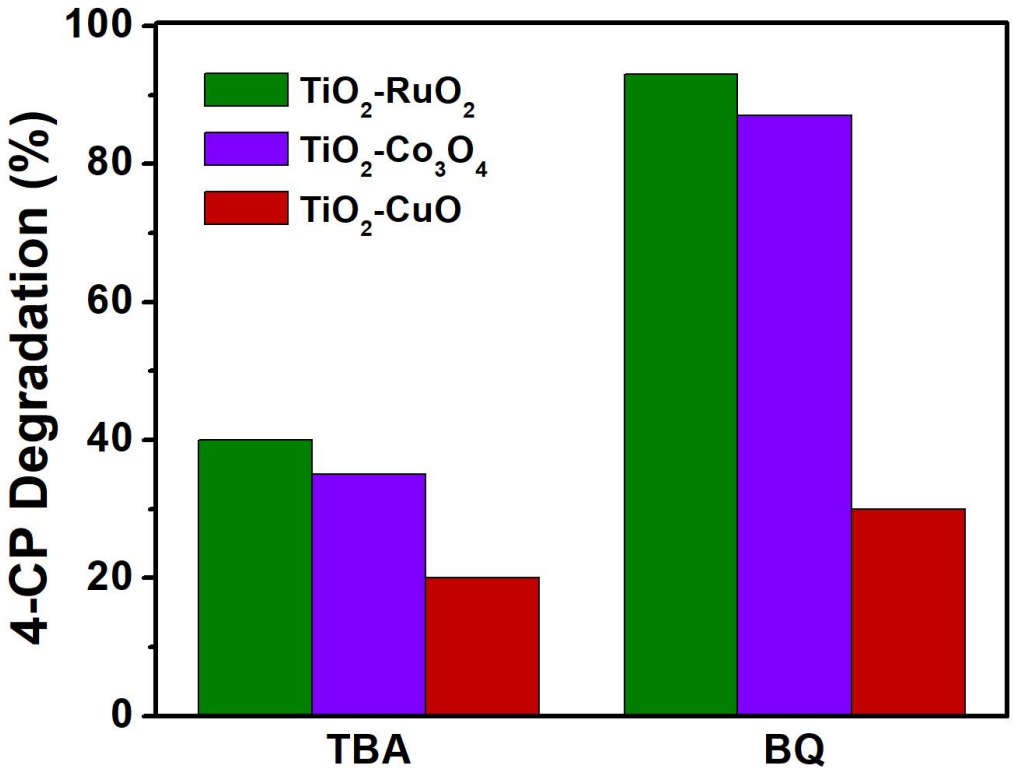

Fig. 7 The effects of electrons and holes scavengers on the photcatalytic degradation of 4-CP over the synthesized heterostructures.

Conclusions:

TiO_2-RuO_2, TiO_2-CuO, and TiO_2-Co_3O_4 heterostructures have been fabricated by a facile hydrothermal method. The heterostructures formation was confirmed by XRD, EDX and FTIR analyses. The solar driven photocatalytic activity of the heterostructures synthesized was examined through the degradation of a colorless model 4-CP under sunlight irradiation. The photodegradation activity was found to follow the trend of TiO_2-CuO>TiO_2-Co_3O_4> TiO_2-RuO_2> TiO_2. It was found that charge migration pathway in TiO_2-RuO_2 and TiO_2-Co_3O_4 follows heterojunction approach which negatively affects the redox potential of the photogenerated electrons and thereby their photocatalytic activity. The drastic enhancement in the photocatalytic activity of TiO_2 has been attributed to the direct Z-scheme charge migration in which the electrons and hole migrate to CB/ VB with the highest redox potential.

Acknowledgement:

This work is supported under UGC-UPE project Govt. of India. Thanks to FE-SEM work at, Mangalore University, India.

Reference:

[1] Zhang, Y., Jiang, Z., Huang, J., Lim, Y.W.L., Li, W., Deng, J., et al., 2015. Titanate and Titania Nanostructured Materials for Environmental and Energy Applications: A Review, RSC Adv. **5**: 79479–79510.

[2] Yang, Y., Niu, S., Han, D., Liu, T., Wang, G. and Li, Y., 2017. Progress in Developing Metal Oxide Nanomaterials for Photoelectrochemical Water Splitting, Adv. Energy Mater. 7: 1–26.

[3] Scushing, S.K., Meng, F., Zhang, J., Ding, B., Chen, C.K., Chen, C.J., et al., 2017. Effects of Defects on Photocatalytic Activity of Hydrogen-Treated Titanium Oxide Nanobelts, ACS Catal. **7**: 1742–1748.

[4] Ou, H.H. and Lo, S.L., 2007. Review of titania nanotubes synthesized via the hydrothermal treatment: Fabrication, modification, and application, Sep. Purif. Technol. **58**: 179–191.

[5] Liu, N., Chen, X., Zhang, Z. and Schwank, J.W., 2017. A review on TiO2-based nanotubes synthesized via hydrothermal method: Formation mechanism, structure modification, and photocatalytic applications, Catal. Today. **225**: 34–51.

[6] Cao, T., Li, Y., Wang, C., Shao, C. and Liu, Y., 2011. A facile in situ hydrothermal method to $SrTiO_3/TiO_2$ nanofiber heterostructures with high photocatalytic activity. Langmuir, **27**(6): 2946-2952

[7] Vinodgopal, K., Bedja,I. and Kamat, P.V., 1996. Nanostructured Semiconductor Films for Photocatalysis. Photoelectrochemical Behavior of SnO_2/TiO_2 Composite Systems and Its Role in Photocatalytic Degradation of a Textile Azo Dye, Chem. Mater. **8** (8) :2180-2187

[8] Shifu, C., , Sujuan, Z., Wei, L. and Wei. Z., 2008. Preparation and activity evaluation of p–n junction photocatalyst NiO/TiO2, Journal of Hazardous Materials **155**(1-2): 320-326

[9] Reza Gholipour, M., Dinh, C.-T., Béland, F. and Do, T.-O., 2015. Nanocomposite heterojunctions as sunlight-driven photocatalysts for hydrogen production from water splitting, Nanoscale**. 7**: 8187–8208.

[10] Marschall, R., 2014. Semiconductor composites: Strategies for enhancing charge carrier separation to improve photocatalytic activity, Adv. Funct. Mater. **24**: 2421–2440.

[11] Bessekhouad, Y., Robert, D. and Weber J-V., 2005. Photocatalytic activity of Cu_2O/TiO_2, Bi_2O_3/TiO_2 and $ZnMn_2O_4/TiO_2$ heterojunctions, Catalysis Today **101** (3-4):315-321

[12] Guo, L., Yang, Z., Marcus, K., Li, Z., Luo, B., Zhou, L., et al., 2017. MoS_2 /TiO_2 heterostructures as nonmetal plasmonic photocatalysts for highly efficient hydrogen evolution, Energy Environ. Sci. **99352**: 0–10.

[13] Dai, G., Liu, S., Liang, Y. and Luo, T., 2013. Synthesis and enhanced photoelectrocatalytic activity of p-n junction Co_3O_4/TiO_2 nanotube arrays, Appl. Surf. Sci. **264** : 157–161.

[14] Ishimaki, K., Uchiyama, T., Okazaki, M., Lu, D., Uchimoto, Y. and Maeda, K., 2018. Influence of TiO_2 Support on Activity of Co_3O_4 /TiO_2 Photocatalysts for Visible-Light Water Oxidation, Bull. Chem. Soc. Jpn. **91:** 486–491

[15] Tian, J., Hu, X., Wei, N., Zhou, Y., Xu, X., Cui, H., et al., 2016. RuO_2/TiO_2 nanobelt heterostructures with enhanced photocatalytic activity and gas-phase selective oxidation of benzyl alcohol, Sol. Energy Mater. Sol. Cells. **151**:7–13.

[16] Lee, S.S., Bai, H., Liu, Z. and Sun, D.D., 2013. Novel-structured electrospun TiO_2/CuO composite nanofibers for high efficient photocatalytic cogeneration of clean water and energy from dye wastewater, Water Res. **47** : 4059–4073.

[17] Zhou, P., Yu, J. and Jaroniec, M., 2014. All-solid-state Z-scheme photocatalytic systems, Adv. Mater. **26**:4920–4935.

[18] Low, J.,Jiang, C.,Cheng, B.,Wageh, S., Al-Ghamdi, A.A. and Yu, J., 2017. A Review of Direct Z-Scheme Photocatalysts, Small Methods. **1**:1700080.

[19] Qi, K., Cheng, B., Yu, J. and Ho, W., 2017. A review on TiO2-based Z-scheme photocatalysts, Chinese J. Catal. **38**:1936–1955.

[20] Hezam, A., Namratha, K., Ponnamma, D., Drmosh, Q.A., Saeed, A.M.M., Cheng, C., et al., 2018.

Direct *Z* -Scheme Cs_2 O–Bi_2 O_3 –ZnO Heterostructures as Efficient Sunlight-Driven Photocatalysts, ACS Omega. **3** :12260–12269.

[21] Xu, Q., Zhang, L., Yu, J., Wageh, S., Al-Ghamdi, A.A. and Jaroniec, M., 2018. Direct Z-scheme photocatalysts: Principles, synthesis, and applications, Materials Today, **21**(10):1042-1063

[22] Jo, W.K., Kumar, S., Isaacs, M.A., Lee, A.F. and Karthikeyan, S., 2017. Cobalt promoted TiO2/GO for the photocatalytic degradation of oxytetracycline and Congo Red, Appl. Catal. B Environ. **201**: 159–168.

[23] Malwal, Deepika, and Gopinath, P., 2016. Enhanced photocatalytic activity of hierarchical three dimensional metal oxide@ CuO nanostructures towards the degradation of Congo red dye under solar radiation, *Catalysis Science & Technology* **6**(12): 4458-4472.

[24] Kuang,,K., Tao Li, T., Chen, Sheng Mao Zhang, Li Li Zhang, and Yu Xin Zhang, 2015. "Hierarchical $Cu_2O/CuO/Co_3O_4$ core-shell nanowires: synthesis and electrochemical properties." *Nanotechnology* **26**(30): 304002.

[25] Dong, C., Xiao, X., Chen, G., Guan, H., Wang, Y., 2015. Morphology control of porous CuO by surfactant using combustion method, *Applied Surface Science* **349**: 844-848.

[26] Chen, I.L., Chen, T.Y., Hu,C.C., Lee, C.H., 2013. Thermal-induced growth of RuO2 nanorods from a binary Ru-Ti oxide composite and alteration in supercapacitive characteristics, J. Mater. Chem. A. **1**:2039–2049.

[27] Hezam, A., Namratha, K., Drmosh, Q.A., Yamani, Z.H. and Byrappa, K., 2017. Synthesis of heterostructured Bi2O3–CeO2–ZnO photocatalyst with enhanced sunlight photocatalytic activity, Ceram. Int. **43**:5292–5301.

[28] Hezam, A., Namratha, K., Drmosh, Q.A., Chandrashekar, B.N., Sadasivuni, K.K., Yamani, Z.H., et al., 2017. Heterogeneous growth mechanism of ZnO nanostructures and the effects of their morphology on optical and photocatalytic properties, CrystEngComm. **19**:3299–3312.

[29] Hezam, A., Namratha, K., Drmosh, Q.A., Chandrashekar, B.N., Jayaprakash, G.K., Cheng, C., et al., 2018. Electronically semitransparent ZnO nanorods with superior electron transport ability for DSSCs and solar photocatalysis, Ceram. Int. **44**:7202–7208.

[30] Hezam, A., Namratha, K., Drmosh, Q.A., Ponnamma, D., Nagi Saeed, A.M., Ganesh, V., et al., 2018. Direct Z-scheme Cs_2O-Bi_2O_3-ZnO heterostructures for photocatalytic overall water splitting, J. Mater. Chem. A. **6** : 21379–21388.

[31] Hezam, A., Namratha, K., Drmosh, Q.A., Lakshmeesha, T.R., Srikantaswamy, S. and Byrappa, K., 2018. The correlation among morphology, oxygen vacancies and properties of ZnO nanoflowers, J. Mater. Sci. Mater. Electron. **29**:13551–13560.

[32] Bai, S., Liu, H., Luo, R., Chen, A. and Li. D., 2014. $SnO_2Co_3O_4$ p–n Heterostructures fabricated by electrospinning and mechanism analysis enhanced acetone sensing, *RSC Advances* **4**(108): 62862-62868.

[33] Patil, R., Sarika K., Naphade, R and Ogale, S., 2014. Low temperature grown $CuBi_2O_4$ with flower morphology and its composite with CuO nanosheets for photoelectrochemical water splitting, *Journal of Materials Chemistry A* **2**(10): 3661-3668.